Influenza A viruses balance ER stress with host protein synthesis shutoff

Beryl Mazel-Sanchez[a], Justyna Iwaszkiewicz[b,1], Joao P. P. Bonifacio[a,1], Filo Silva[a], Chengyue Niu[a], Shirin Strohmeier[c], Davide Eletto[d], Florian Krammer[c], Gene Tan[e,f], Vincent Zoete[b], Benjamin G. Hale[d], and Mirco Schmolke[a,2]

[a]Department of Microbiology and Molecular Medicine, University of Geneva, 1211 Geneva, Switzerland; [b]Molecular Modelling Group, Swiss Institute of Bioinformatics, 1015 Lausanne, Switzerland; [c]Department of Microbiology, Icahn School of Medicine at Mount Sinai, New York, NY 10029; [d]Institute of Medical Virology, University of Zürich, 8057 Zürich, Switzerland; [e]Infectious Diseases, J. Craig Venter Institute, La Jolla, CA 92037; and [f]Division of Infectious Diseases, Department of Medicine, School of Medicine, University of California San Diego, La Jolla, CA 92093

Edited by Yoshihiro Kawaoka, University of Wisconsin–Madison, Madison, WI, and approved July 15, 2021 (received for review December 9, 2020)

Excessive production of viral glycoproteins during infections poses a tremendous stress potential on the endoplasmic reticulum (ER) protein folding machinery of the host cell. The host cell balances this by providing more ER resident chaperones and reducing translation. For viruses, this unfolded protein response (UPR) offers the potential to fold more glycoproteins. We postulated that viruses could have developed means to limit the inevitable ER stress to a beneficial level for viral replication. Using a relevant human pathogen, influenza A virus (IAV), we first established the determinant for ER stress and UPR induction during infection. In contrast to a panel of previous reports, we identified neuraminidase to be the determinant for ER stress induction, and not hemagglutinin. IAV relieves ER stress by expression of its nonstructural protein 1 (NS1). NS1 interferes with the host messenger RNA processing factor CPSF30 and suppresses ER stress response factors, such as XBP1. In vivo viral replication is increased when NS1 antagonizes ER stress induction. Our results reveal how IAV optimizes glycoprotein expression by balancing folding capacity.

ER stress | influenza virus | neuraminidase | NS1 | CPSF30

Viruses are obligate intracellular parasites, which rely entirely on the host cell machinery for synthesis of viral proteins. Both host and viral surface glycoproteins are synthesized in the cytosol and are then quickly directed to the endoplasmic reticulum (ER). Here, they are folded by ER chaperones and can undergo posttranslational modification with the addition of N-linked glycosylations or disulphide bonds (1). The amount of free ER chaperones and ER resident enzymes required for posttranslational modification limit the capacity of the ER to fold newly synthesized proteins. Under physiological conditions, the ER folding capacity is adjusted to the cell's demand. However, during viral infection, the sudden need to process large amounts of viral glycoproteins can drive the ER beyond its folding capacity. In such cases, unfolded and/or misfolded proteins accumulate in the ER, causing ER stress and triggering the unfolded protein response (UPR). The ER chaperone binding immunoglobulin protein (BiP), a member of the heat shock protein family, is a master sensor of the UPR that recognizes misfolded protein accumulation (2–4). Low levels of misfolded proteins do not exceed the steady-state pool of BiP in the ER. In this steady state, a proportion of BiP is bound by the ER transmembrane sensors inositol-requiring enzyme 1α (IRE1α), protein kinase R-like ER kinase (PERK), and activated transcription factor 6 (ATF6) and keeps them in an inactive state. However, accumulation of misfolded proteins recruits BiP away from all three sensors, which triggers three specific signaling cascades in the cytoplasm that, in concert, aim to restore proteostasis by increasing the amount of ER chaperones (including BiP), as well as ER size (2, 5). For example, when activated, IRE1α dimerizes, autophosphorylates, and triggers the specific cytoplasmic splicing of X-box binding protein 1 (XBP1) messenger RNA (mRNA). The spliced XBP1 (sXBP1) mRNA is translated into a functional transcription factor (6) responsible for activation of UPR-related genes (7, 8). In the case the UPR fails to return the balance between ER folding machinery and glycoprotein production, apoptosis will be induced (9). While apoptosis of the host cell may not be a key aim of the virus, one could imagine that expansion of the folding capacity in the ER would be beneficial for production of viral progeny.

Influenza A viruses (IAV) are segmented negative-sense RNA viruses that infect human airway epithelial cells. Like other viruses, they rely heavily on the ER function to produce their two envelope glycoproteins, hemagglutinin (HA) and neuraminidase (NA), as well as the transmembrane protein M2. The ER maturation steps of both IAV HA and NA were extensively studied (10–13). For both HA and NA, the folding of the monomer is guided by the ER lectin chaperones calnexin (CNX) and calreticulin (CRT), which are recruited via N-linked glycosylation (14). The monomer is then stabilized by intramolecular disulphide bonds (15). For HA, trimers are formed in the ER or at the ER–Golgi interface (16). For NA, dimers are first formed in the ER by intermolecular disulfide bonds. These dimers are then assembled to tetramers, a step requiring glycosylation of NA as well as conformational changes both in the transmembrane domain and the head domain (17, 18). During the maturation process of glycoproteins, host proteins play the role of sentinels

Significance

As intracellular parasites, viruses depend on the host cell machinery to produce and fold viral proteins. Because the capacity to fold proteins is limited, excessive viral translation of glycoproteins leads to ER stress. Unresolved ER stress drives host cells into apoptosis. We identify the expression of neuraminidase as the molecular source of influenza A virus–induced ER stress. The virus naturally balances it by the limitation of host protein production through the viral host shutoff protein NS1. The host cell mounts an unfolded protein response, creating additional protein folding reserves. Ultimately, the virus uses the stress-induced protein production capacities of the host cell to its own replication advantage.

Author contributions: B.M.-S., J.I., V.Z., and M.S. designed research; B.M.-S., J.I., J.P.P.B., F.S., C.N., V.Z., and M.S. performed research; S.S., D.E., F.K., G.T., and B.G.H. contributed new reagents/analytic tools; B.M.-S., J.I., J.P.P.B., F.S., C.N., V.Z., and M.S. analyzed data; and B.M.-S., J.I., C.N., F.K., B.G.H., and M.S. wrote the paper.

The authors declare no competing interest.

This article is a PNAS Direct Submission.

[1]J.I. and J.P.P.B. contributed equally to this work.

[2]To whom correspondence may be addressed. Email: mirco.schmolke@unige.ch.

This article contains supporting information online at https://www.pnas.org/lookup/suppl/doi:10.1073/pnas.2024681118/-/DCSupplemental.

Published September 3, 2021.

to ensure that all proteins are folded properly before they exit the ER. It is notably the role of the ER chaperone BiP, which can recognize both influenza HA and NA when they are misfolded (19, 20).

IAV infection was previously described to modulate ER stress. According to the literature, the most prominent viral glycoprotein (HA) is responsible for triggering ER stress. Lack of HA glycosylation in pandemic or zoonotic IAV strains has been associated with more ER stress induction in human cells and more immune pathology in whole organism mouse models (21, 22). The literature agrees that IAV activates the IRE1α pathway (23–25), but there is more controversy concerning the PERK and ATF6 pathway (23, 24). Research has focuses on activation of the UPR by IAV. However, to date, no strategies used by IAV to limit ER stress have been described.

Here, we generated IAV strains in a targeted manner that induce either a weak or strong ER stress response following infection. By genetically exchanging the glycoproteins, we show that the viral NA is the master inducer of ER stress and UPR. ER resident amounts of NA and the predicted presence of amino acid stretch recognized by BiP determine the levels of the ER stress response during viral infection. Host cells respond by expanding the ER volume and providing more ER chaperones. We further show that controlling the production of host proteins is essential for the virus to counteract ER stress. This control is achieved by the IAV nonstructural protein 1 (NS1) blocking cleavage-polyadenylation specificity factor 30 (CPSF30) function, a key factor of the cellular polyadenylation complex (26, 27). The NS1 protein of IAV prevents binding of CPSF30 to cellular pre-mRNA, thereby preventing their correct maturation and limiting host protein production (28, 29). This function was initially attributed to antagonism of type I interferon and inflammatory response (30–32). Our results reveal an additional function of NS1 in limiting the host ER stress response to the benefit of IAV replication.

Results

Induction of ER Stress Varies among Viral Isolates. Previous studies showed that IAV activates ER stress. In order to define whether this is a general feature of IAV infection, or limited to certain viral strains, we infected A549 human lung epithelial cells with a panel of representative IAV laboratory strains and clinical isolates. Then we performed a RT-PCR to compare the amount of spliced XPB1 (sXPB1) mRNA. Infection with a high multiplicity of infection (MOI) resulted in similar infection levels between the different IAV strains, as indicated by the presence of comparable amounts of viral nucleoprotein (NP) in cell lysates 8 h postinfection (pi) (Fig. 1 *A*, *Lower*). All viruses, except A/Switzerland/9715293/13-like (H1N1) (CH13) and A/Wyoming/03/2003 (H3N2) (Wyo03), displayed a similar number of infected cells (*SI Appendix*, Fig. S1*A*). Strikingly, levels of the sXBP1 amplicon at the same time point were different (Fig. 1 *A*, graph and *Middle*). Two strains, A/Puerto Rico/8/1934 (H1N1) (PR8) and X31 (a chimeric virus with PR8 internal genes and HA and NA from A/Aichi/2/1968 [H3N2]), induced a significant increase in the amount of sXBP1 mRNA. In contrast A/Viet Nam/1203/2004 (H5N1-HALo) (an engineered low-pathogenic variant) (VN1203), Wyo03, A/Netherlands/602/2009 (pandemic H1N1) (Neth602) and two clinical isolates (A/Hong Kong/2212/10-like (H1N1) (HK10) and CH13 did not trigger splicing of XBP1 mRNA. We furthermore observed a reduction of unspliced XBP1 mRNA, as compared with mock, for cells infected with several IAV strains (*Upper* band Fig. 1 *A*, *Upper* panel). This suggests strain-specific mechanisms regulating expression or degradation of the XBP1 mRNA. In order to rule out kinetic differences in ER stress induction between viruses, we tested XBP1 splicing 4 h and 12 h pi in cells infected with VN1203 or PR8. As for 8 h pi these early and late time points did not reveal XBP1 splicing in VN1203-infected cells (Fig. 1*B*). Notably, transient activation of XBP1 splicing by PR8 infection may suggest a balancing of the cellular and viral responses to ER stress induction. In order to demonstrate that PR8 infection induces a broad ER stress response, while VN1203 does not, we performed qPCR for genes that are up-regulated by the different ER stress sensor (Fig. 1*C*). We picked Erdj4 (IRE1 pathway), BiP (ATF6 pathway) (33), and CHOP and GADD34 [PERK (34) and ATF6 pathway (35)]. We could observe an induction of all genes in PR8-infected cells compared with VN1203-infected cells, thus showing that PR8 infection triggers all three arms of the UPR.

As a reaction to ER stress, cells enhance the folding capacity for glycoproteins by ER volume expansion and increased expression of ER resident chaperones. In order to determine the ER volume in mock versus IAV-infected cells, we analyzed confocal Z-stack images of A549 cells, using the ER resident chaperone BiP (green) as an ER volume marker, and CD44 (red) to define the outer perimeter of each cell. After subtraction of the nuclear volume (blue, DAPI stained), we determined the relative ER volume per cytoplasm volume per cell (Fig. 1 *D* and *E* and *SI Appendix*, Fig. S1 *B* and *C* and Movies S1–S6). We used tunicamycin (Tm) treatment as a positive control to validate our microscopy approach. In the context of PR8 viral infection, the ER volume (compared with mock-treated cells) doubled after 24 h (Fig. 1*D*). No significant differences in ER volume were detectable at the time point of maximum XBP1 splicing (8 h pi) (Fig. 1*D*). The delay between appearances of sXBP1 mRNA at 8 h postinfection as a direct response to ER stress and the increase of the ER volume at 24 h could be explained by the kinetics of the UPR (36). In contrast, in the context of VN1203 viral infection, which did not induce XBP1 mRNA splicing, we did not observe a change in the ER volume compared with mock-treated cells, and this at both 8 h and 24 h postinfection (Fig. 1*E* and *SI Appendix*, Fig. S1*C*).

Our data emphasize that the magnitude of ER stress and the UPR in context of IAV infection is virus strain dependent.

IAV Activates ER Stress in an NA-Dependent Manner. IAV displays two major glycoproteins on its surface, HA and NA, with HA being approximately 10 times more abundant that NA on virions (37). The current literature on IAV-induced ER stress solely focuses on HA as a trigger for ER stress. In order to assess which glycoprotein is the main ER stress inducer, we decided to exchange HA and NA between an IAV isolate, which induces ER stress (PR8) and one, which does not induce it (VN1203). Gene segments for HA and NA were swapped (separately or together) using reverse genetics. In contrast to previous findings, indicating HA as the main protein inducing ER stress, we found that PR8 with HA of VN1203 induces equal amounts of ER stress as PR8 (Fig. 2*A*) upon infection in A549 cells. Importantly, replacement of PR8 NA by VN1203 NA abolished XBP1 splicing after PR8 VN1203 NA infection, thus identifying NA as the inducer of ER stress response. This phenotype correlated well with the expression levels of NA. Of note, we insured that our panN1 antibody displayed equal binding to H5N1 and H1N1 NAs by testing whole cell lysates of cells transfected with plasmid expressing NA tagged with a V5 epitope and compared the panN1 antibody and an anti-V5 antibody (*SI Appendix*, Fig. S2*A*). Notably, the inverse approach (i.e., VN1203 expressing PR8 NA) did not trigger XBP1 splicing despite high amounts of PR8 NA present in the infected cells. This could argue for an additional negative regulation of ER stress by VN1203, but not PR8. In line with these findings, the detection of sXBP1 mRNA by PCR correlates well with the presence of sXPB1 protein as seen by Western blot (WB) (Fig. 2*A*).

In order to strengthen our conclusion that HA is not the glycoprotein inducing ER stress during infection, we took advantage of a recently published recombinant PR8 virus (38). In this virus, the

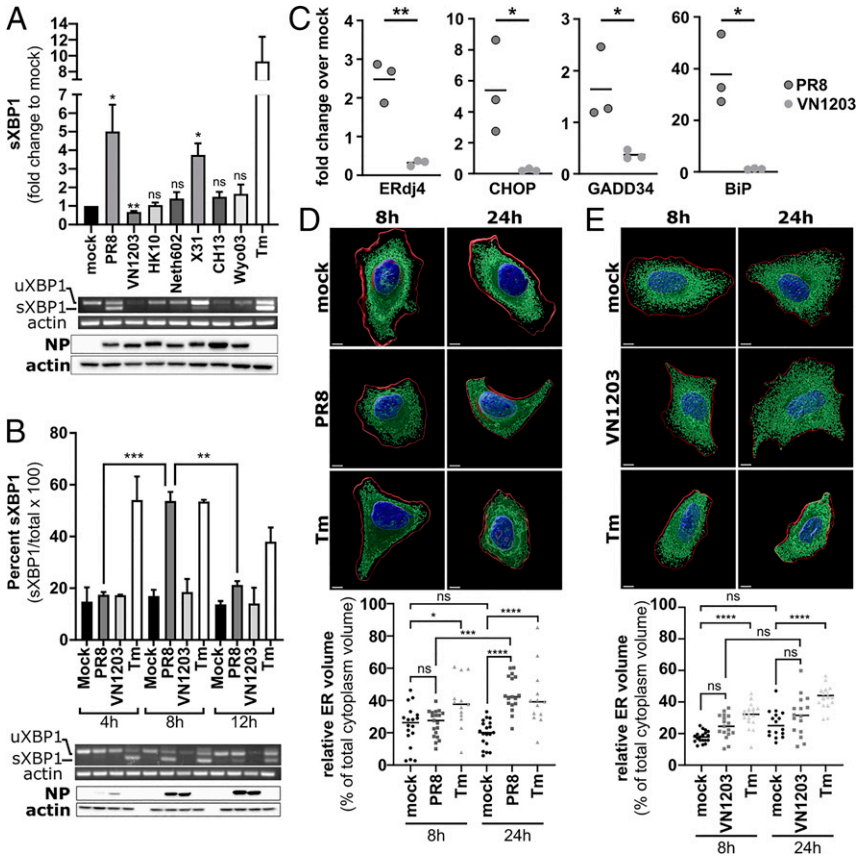

Fig. 1. Induction of ER stress varies among viral isolates. (*A*) A549 cells were infected at an MOI of 5 with the following strains: PR8 (A/Puerto Rico/8/1934 [H1N1]), VN1203 (A/Vietnam/1203/2004 [H5N1]), Neth602 (A/Netherlands/602/2009 [H1N1]), HK10 (A/Hong Kong/2212/10-like 2014 [H1N1]), X31 (PR8 internal genes with HA and NA from A/Aichi/2/1968 [H3N2]), CH13 (A/Switzerland/9715293/13-like 2014 [H3N2]), Wyo03 (A/Wyoming/03/2003 [H3N2]) or treated with PBS (mock) or Tm. Cells were collected 8 h postinfection and analyzed by semiquantitative RT-PCR and WB (for viral protein NP and actin), respectively. The graph represents mean with SD of the densitometry analysis of the sXBP1 mRNA ($n = 3$), and unpaired *t* test was used to compared each sample with mock. (*B*) A549 cells were infected at a MOI of 5 with PR8 and VN1203 or treated with PBS (mock) or Tm. Cells were collected 4 h, 8 h, and 12 h pi and analyzed by semiquantitative RT-PCR and WB. The graph represent means with SD of the densitometry analysis of the sXBP1 cDNA ($n = 2$). Time points were compared using one-way ANOVA with Tukey correction. (*C*) A549 cells were treated with PBS (mock) or infected at a MOI of 5 with PR8 or VN1203. At 8 h postinfection, cells were lysed and RNA was extracted and processed through RT-qPCR analysis for ER stress–related genes (ERdj4, CHOP, GADD34, and BiP). Each graph represents the fold change over mock for the indicated gene. Each dot represents one well and the bar represents the mean. Unpaired *t* test was used to compare viruses. (*D* and *E*) A549 cells were treated with PBS (mock) or Tm or infected at a MOI of 5 with either PR8 (*D*) or VN1203 (*E*). Cells were fixed 8 h and 24 h postinfection and processed for immunofluorescence. Z-stacks were analyzed. Images show 3D rendered representations of representative cells with the ER resident protein BiP in green, the plasma membrane marker CD44 in red, and the nucleus in blue. (Scale bars [*Bottom Left*], 5 μm.) The graph below shows a quantification of the ER volume in an individual cell. Values are expressed in percentage of the cytoplasm volume. Each dot represents one cell and the median is represented by a line. The medians of each column were compared using one-way ANOVA with Turkey correction. ns $P > 0.05$, $*P \leq 0.05$, $**P \leq 0.01$, $***P \leq 0.001$, $****P \leq 0.0001$.

untranslated promoter-containing regions were swapped between the HA and the NA segment (PR8 swap). In A549 cells infected with this virus, we observed a drastic reduction in the amount of HA, while the total expression of NA was only slightly increased (Fig. 2*B*). Importantly, the level of ER stress induced by PR8 swap was similar to the one induced by PR8. This isogenic control allowed us to rule out HA as the glycoprotein inducing ER stress.

In order to circumvent the complexity of viral replication, we individually expressed a panel of V5-tagged NAs from different viral strains using transfection. In this model system, we used a luciferase reporter activated by an IRE1α-dependent cleavage of the XBP1 splicing motif (39). The induction of this reporter was also strain dependent, revealing that PR8 NA, but not VN1203 NA, is an inducer of ER stress when expressed in the absence of infection. Furthermore, we identified that induction can be triggered by a panel of NAs from a range of different IAVs, but this does not correlate with the amount of NA present in the cell (Fig. 2*C*). This result implies that specific characteristics of NA contribute to ER stress induction.

Furthermore, NA of Cal09 (whose amino acid sequence is 99.8% similar to the one of Neth602) was a strong inducer of the UPR when expressed individually (Fig. 2*C* and *SI Appendix*, Fig. S2*B*), while the full virus did not cause XBP1 splicing (Fig. 1*A*). These observations argue for the presence of a specific viral inhibitor of ER stress that is encoded by some viral isolates.

NA Activity and Glycosylation Pattern Are Not Determinants of ER Stress Induction. In order to better understand what defines the NA-dependent ER stress induction, we compared different properties of PR8 NA (as a strong inducer of XBP1 splicing and ATF6 activation) and VN1203 NA (as a noninducer of XBP1 splicing and a weak inducer of ATF6) (*SI Appendix*, Fig. S2*B*). First, we tested the impact of glycosylation, since increased glycosylation of the major surface antigen HA was associated with reduced ER stress induction (21). Based on the glycosylation motif N-X-S/T, PR8 NA is predicted to be glycosylated at five positions (N44, N58, N73, N131, and N220), while VN1203 NA is predicted to be glycosylated at three positions (N73, N131, and

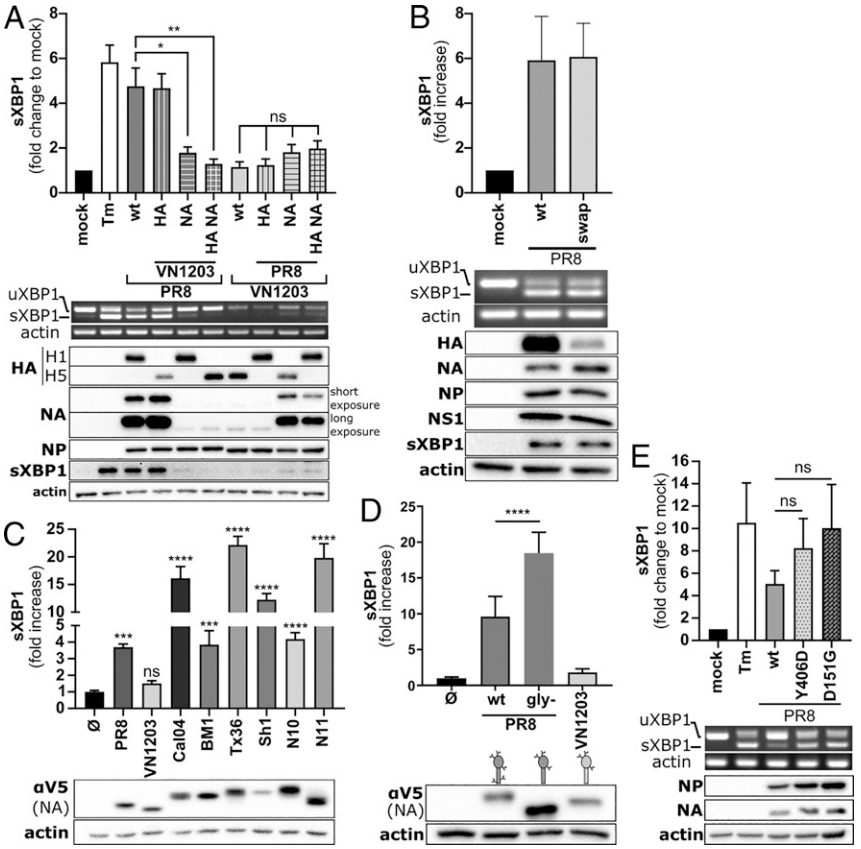

Fig. 2. IAV activates ER stress in a NA-dependent manner. (*A*) A549 cells were infected at a MOI of 5 with indicated WT and chimeric viruses or treated with PBS (mock) or Tm. Cells were collected 8 h postinfection and lysates were analyzed by semiquantitative RT-PCR and WB for viral proteins (HA, NA, and NP) and cellular proteins (sXBP and actin). The graph represents mean with SD of the densitometry analysis of the sXBP1 cDNA ($n = 3$) and one-way ANOVA with Dunnett correction was used to compared each mutant virus with its WT counterpart. (*B*) A549 cells were treated with PBS (mock) or infected at a MOI of 5 with PR8 or PR8 swap UTR viruses. Cells were collected 8 h postinfection and lysates were analyzed by semiquantitative RT-PCR and WB for viral proteins (HA, NA, NP, and NS1) and cellular proteins (sXBP1 and actin). The graph represents mean with SD of the densitometry analysis of the sXBP1 cDNA ($n = 3$). (*C*) The 293T cells were transfected with pFLAG-XBP1u-FLuc and pCAGGS empty vector (Ø) or pCAGGS encoding the V5-tagged neuraminidase from different viruses: PR8 (A/Puerto Rico/8/1934), VN1203 (A/Viet Nam/1203/2004), Cal04 (A/California/04/2009), BM1 (A/Brevig Mission/1/1918), Tx36 (A/Texas/36/1991), Stx4199 (A/Swine/Texas/4199-2/1998), Sh1 (A/Shanghai/01/2013), N10 (A/little yellow-shouldered bat/Guatemala/153/2009 [H17N10]), and N11 (A/flat-faced bat/Peru/033/2010 [H18N11]). Cells were lysed 24 h posttransfection. Lysates were subjected to luciferase activity measurement and WB analysis using anti-V5 antibody. The graph represents the mean fold increase luciferase activity normalized to mock with SD of triplicate ($n = 3$) and one-way ANOVA with Dunnett correction was used to compare each condition with mock. (*D*) The 293T cells were transfected with pFLAG-XBP1u-FLuc and pCAGGS empty vector (Ø) or pCAGGS encoding different V5-tagged neuraminidases: PR8 NA, PR8 NA glycosylations mutant (gly-) and VN1203 NA. Cells were lysed 24 h posttransfection. Lysates were subjected to luciferase activity measurement and WB analysis using anti-V5 antibody. Graphs represent the mean fold increase luciferase activity normalized to mock with SD of triplicate ($n = 5$). Unpaired *t* test was used to compare the two PR8 viruses. (*E*) A549 cells were infected at a MOI of 5 with PR8 and PR8 neuraminidase mutants as indicated or treated with PBS (mock) or Tm. Cells were collected 8 h postinfection and analyzed by semiquantitative RT-PCR and WB. The graph represents mean fold change normalized to mock with SD of the densitometry analysis of the sXBP1 cDNA ($n = 3$), and one-way ANOVA with Dunnett correction was used to compared each mutant virus with its WT counterpart. ns $P > 0.05$, $*P \leq 0.05$, $**P \leq 0.01$, $***P \leq 0.001$, $****P \leq 0.0001$.

N220) (PR8 NA numbering). By removing two predicted glycosylation sites in PR8 NA (N44A and N58A), we mimicked the predicted glycosylation pattern of VN1203 NA. This PR8 NA glycosylation mutant migrated faster in sodium dodecyl (lauryl) sulfate–polyacrylamide gel electrophoresis (SDS-PAGE) under reducing conditions, indicating that the predicted sites are indeed glycosylated. In contrast to published findings on HA glycosylation (21), removal of glycosylation sites enhanced the specific capacity of PR8 NA to induce ER stress (Fig. 2*D*). This could be explained by the increased amount of NA present in the cell and/or by potential misfolding of the mutant PR8 NA.

Next, we turned to possible differences in the enzymatic function of the two neuraminidases. Using an enzyme-linked assay, we compared the sialidase activities of purified, insect cell–expressed PR8 NA and VN1203 NA. In this assay, PR8 NA displayed a greater specific sialidase activity (*SI Appendix*, Fig. S2 *C*, *Top*). We obtained the same result using whole virions normalized to the same plaque-forming units (pfu) (*SI Appendix*, Fig. S2 *C*, *Lower*). However, introduction of amino acid substitutions in the catalytic site of PR8 NA (D151G or Y406D), which lower enzymatic activity (40, 41), did not reduce ER stress induction during PR8 infection (Fig. 2*E*). In order to independently corroborate this result, we took advantage of the recently identified bat influenza A virus neuraminidases N10 and N11, which are devoid of intrinsic sialidase activity (42, 43). The two bat IAV NAs were strong inducers of ER stress when overexpressed (Fig. 2 *C*, *Right*). Taken together, these results argue against both glycosylation pattern and neuraminidase activity being defining features of NA responsible for ER stress induction.

NA Amount in the ER and BiP Binding Correlate with ER Stress Induction. Up to this point, we only accounted for total NA amounts. However, ER stress would presumably depend on ER-localized NA. Indeed, accumulation of misfolded or unfolded

viral glycoproteins is proposed to lead to ER stress (25, 44). In general, misfolded glycoproteins in the ER are actively transported from the ER to the cytoplasm by the ERAD machinery, where they undergo proteasomal degradation (45). To test the possibility that NA overload in the ER is responsible for ER stress, we blocked the retrograde ER-cytoplasmic transport of misfolded proteins with kifunensine and measured ER stress induction using the XBP1 luciferase reporter assay (Fig. 3*A*) (46). Cells transfected with an empty plasmid and treated with kifunensine did not show any increase in XBP1 splicing. This shows that the ER of cells in a physiological state is not under stress, even if the ERAD pathway is blocked. However, following overexpression of PR8 NA, we observed a dose-dependent increase of XBP1 splicing. This effect was clearly increased by kifunensine. In contrast, overexpression of VN1203 NA did not cause ER stress in the presence of kifunensine. However, the baseline expression of this NA was substantially lower than that of PR8. This result confirms that for NAs with the intrinsic capacity to induce ER stress, the ER resident portion of the protein constitutes the main trigger.

BiP is a key sensor for unfolded proteins in the ER lumen. We used the method developed by Schneider et al. to predict the potential BiP binding site in different NA proteins (47). BiPPred evaluates the BiP binding probability and gives a forward and reverse score for each consecutive 7 amino acid stretch of a given protein sequence. The probability of a given peptide being a BiP binding site is attributed a score between 0 (minimal) and 1 (maximal). In our analysis, we counted the total number of peptides scoring 0.8 or higher. We hypothesized two potential scenarios, in which 1) NA is fully unfolded and accessible to BiP or 2) only unstructured regions are bound by BiP. Obviously, both scenarios could take place in parallel during infection. When looking at the whole protein sequence of NA (scenario 1), we established that there is a significant correlation between the total number of peptides scoring equal or higher than 0.8 and the capacity of the protein to induce ER stress (Fig. 3*B*). However, glycoproteins are rapidly folded upon synthesis at the ER membrane; thus we also evaluate the number of peptides recognized by BiP within the intrinsically disordered or exposed part of NA, which are the N-terminal 75 to 95 amino acids and the internal exposed loop whose sequences are described in *SI Appendix*, Tables S1 and S2, respectively (scenario 2). We chose to focus on those two features of the NA because, according to the model, they should be exposed even when the NA monomer is fully folded. As for the full NA sequence, we could observe a good correlation between the number of peptides with a high probability of BiP binding and the induction of ER stress (Fig. 3*C*). Accumulation of NA in the ER could at a certain point

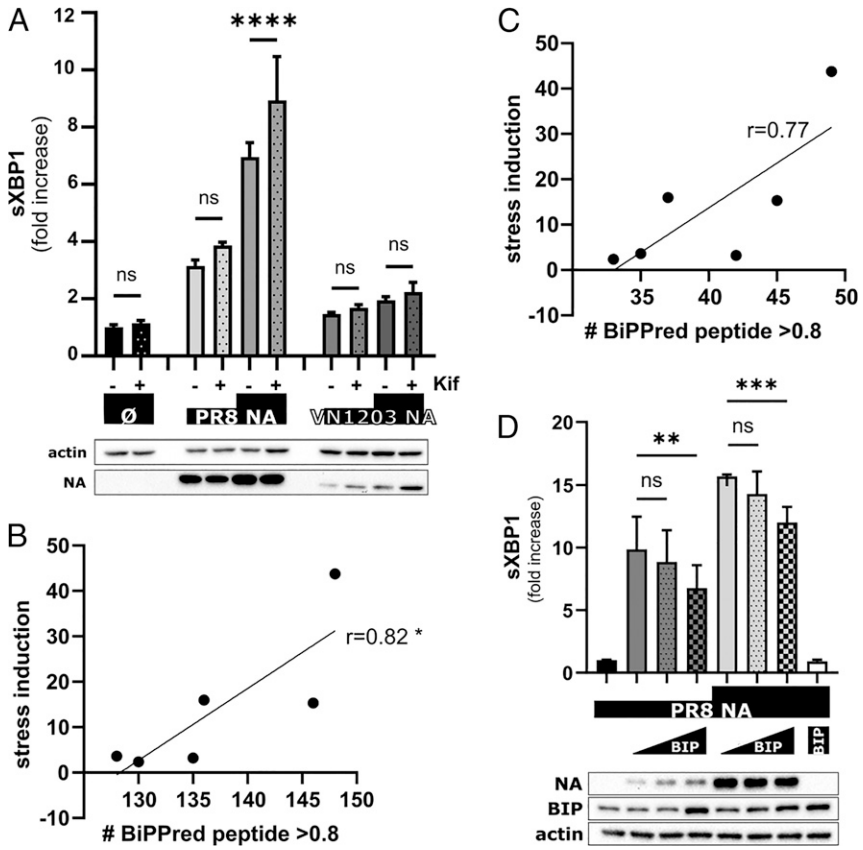

Fig. 3. NA amount in the ER and NA/BiP interaction play a role in ER stress induction. (*A*) The 293T cells were transfected with pFLAG-XBP1u-FLuc and pCAGGS empty vector (Ø) or pCAGGS encoding V5-tagged PR8 NA at different amounts. At 6 h posttransfection, cells were treated with kifunensine for 24 h and lysed. Lysates were subjected to luciferase activity measurement and WB analysis using an anti-V5 antibody. Graphs represent the mean fold increase over mock with SD of technical triplicates ($n = 2$). One-way ANOVA with Turkey correction was used for statistical analysis. (*B* and *C*) Correlation between predict differences in the number of peptide with a BiPPred score higher than 0.8 for the whole NA (*B*) or the internal loop and the N terminus of NA (*C*) and specific induction of ER stress (normalized to NA amount). (*D*) The 293T cells were transfected with pFLAG-XBP1u-FLuc, pCAGGS empty vector (Ø), or pCAGGS encoding V5-tagged PR8 NA and pcDNA3.1(+)-GRP78/BiP. Cells were lysed 24 h posttransfection and lysates were subjected to luciferase activity measurement and WB analysis using an anti-V5 and anti-BiP antibody. Graphs represent the mean Firefly luciferase activity normalized to mock with SD of technical triplicates ($n = 2$). One-way ANOVA with Turkey correction was used for statistical analysis. ns $P > 0.05$, *$P \leq 0.05$, **$P \leq 0.01$, ***$P \leq 0.001$, ****$P \leq 0.0001$.

exceed the pool of free BiP. We thus supplemented BiP to compensate NA overload in the ER (Fig. 3*D*). Overexpression of BiP alone did not modify the basal level of XBP1 reporter activity. However, in combination with PR8 NA overexpression, XBP1 splicing was decreased in a dose-dependent manner. These experiments show that NA accumulation in the ER triggers a stress response, with BiP being the limiting host factor. Taken together, these data suggest an important role for NA accumulation and BiP recognition in the induction of ER stress.

NS1-Induced Shutoff Inhibits ER Stress Induction. Up to this point, two findings suggested the presence of a virus-encoded inhibitor of ER stress responses: first, chimeric VN1203 displaying PR8 NA did not induce XBP1 splicing; and second, while exogenously expressed Cal04 NA was a potent ER stress inducer, infection with a closely related virus (A/Netherlands/602/2009) did not cause XBP1 splicing in A549. Notably, we found that both PR8 and X31 viruses induced XBP1 splicing in infected A549. X31 is a chimeric virus that harbors HA and NA from A/Aichi/2/1968 (H3N2), while having the internal genes of PR8. In contrast, the clinical H3N2 isolate did not trigger ER stress. This points toward the existence of a viral inhibitor encoded by one or more of the remaining IAV segments 1, 2, 3, 5, 7, or 8, and which is potentially nonfunctional in PR8.

We hypothesized that one way of reducing the combined burden of host and viral protein folding on the ER is to reduce overall host protein synthesis. Two viral proteins, PA-X and NS1, have been particularly implicated in regulating general host protein expression, the so-called host protein shutoff. PA-X is an alternative translation product from segment 3 mRNA, sharing the endonuclease domain with PA, which resides in the cytoplasm and stress granules. PA-X was proposed to cleave host mRNAs (48, 49). The nonstructural protein 1 (NS1) targets CPSF30 and prevents polyadenylation of host mRNAs in the nucleus, which ultimately leads to mRNA degradation (28). When testing a PA frameshift mutant of PR8 and VN1203, we did not observe an increase in ER stress induction in infected A549s, as indicated by sXBP1 both at the mRNA level and protein level (Fig. 4*A*). These data suggest that PA-X is not a major antagonist of the IAV-induced ER stress response.

We next focused on the NS1 protein and its ability to bind CPSF30. Strikingly, NS1 of PR8 is known to lack the capacity to bind CPSF30 and block mRNA maturation, while the NS1 from VN1203 is a strong inhibitor of CPSF30, and the NS1 from Cal04 is partially functional, but largely inefficient (31, 32). In order to test specifically whether exogenous expression of NS1 relieves ER stress, we used a luciferase reporter assay for XBP1 splicing in cells treated or not with tunicamycin, and transfected a panel of NS1 constructs as indicated, to represent the different NS1/CPSF30 binding phenotypes (Fig. 4*B*). First, we observed that NS1 overexpression itself does not lead to induction of ER stress and we observed that, as previously described, NS1 inhibits its own expression when binding to CPSF30 (32). In addition, we found that the ability of NS1 to bind CPSF30 correlated well with its capacity to inhibit tunicamycin-induced ER stress: PR8 NS1 was unable to limit tunicamycin-induced ER stress despite expressing very well, while VN1203 NS1 was a potent inhibitor and Neth602 NS1 had a small effect (Fig. 4*B*). We observed the same correlation when testing a panel of NS1 proteins (Fig. 4*C* and *SI Appendix*, Table S3).

In order to confirm this correlation in functional tests, we introduced the NS1 binding mutations into the respective viruses using reverse genetics. We introduced nucleotide changes (*SI Appendix*, Table S3) into the NS segment in order to either induce binding of NS1 to CPSF30 or disrupt this ability. We generated two mutants that gained the ability to bind to CPSF30, i.e., PR8 NS1^{+} and Neth602 NS1^{+} and two mutants that lost the ability to bind CPSF30, i.e., VN1203 NS1^{-} and Neth602 NS1^{-}. We used these viruses to confirm the gain or loss of binding of NS1 to CPSF30. The 293T cells expressing a Flag-tagged human CPSF30 protein were infected with the different viruses, i.e., PR8, PR8 NS1^{+}, VN1203, VN1302 NS1^{-}, Neth602, Neth602 NS1^{-} and Neth602 NS1^{+}. Cell lysates were subjected to immunoprecipitation (IP) using anti-Flag affinity beads. The Flag-CPSF30/NS1 complexes were analyzed by WB (Fig. 4*D*) and the relative amount of NS1 bound to CPSF30 was quantified (Fig. 4*E*). We observed that the NS1^{+} mutants, which have the amino acid sequence associated with CPSF30 binding phenotype, indeed bind more to CPSF30 than their cognate NS1 wild type (WT). On the other hand, NS1^{-} mutants bind less to CPSF30 than NS1 WT. Of note the presence of viral PA and NP during infection stabilizes the NS1/CPSF30 complex (50), which could explain the residual binding observed for PR8. We corroborated the binding data functionally with a surrogate assay for NS1-mediated host protein synthesis shutoff. Previous data have shown the link between efficient control of reporter gene expression and efficient binding of NS1 to CPSF30 (32). A constitutively active Gaussia luciferase reporter was coexpressed with each of the different NS1, and luciferase activity was measured 24 h posttransfection. We observed an enhanced expression of Gaussia luciferase with NS1^{-} mutants and a suppressed expression with NS1^{+} mutants (Fig. 4*F*). These data confirm that the mutations we introduced are involved in NS1/CPSF30 binding and more generally in host cell mRNA polyadenylation.

Next, we tested the ability of the NS1 mutants to inhibit tunicamycin-induced ER stress compared with their cognate NS1. In accordance with our pulldown experiemnt, the NS1 CPSF30 binding "gain-of-function" mutant of PR8 (NS1^{+}) blocked XBP1 reporter activation (Fig. 4*G*). Inversely, loss of CPSF30 binding in VN1203 NS1 (NS1^{-}) abolished its inhibitory function on XBP1 splicing (Fig. 4*H*). Lastly, Neth602 NS1 displays an intermediate CPSF30 binding phenotype, and introduction of a strong CPSF30 binding interface increases its XBP1 antagonistic function, while introduction of a weak interface removes this capacity (Fig. 4*I*).

Then, we tested the ability of NS1 to inhibit or not the induction of ER stress in the context of infection. We could recapitulate the effect in A549 infected with PR8: when PR8 NS1 can functionally bind CPSF30, ER stress induction in infected cells is inhibited when measuring levels of sXBP1 by RT-PCR (Fig. 4*J*), despite similar expression of the ER stress inducing PR8 NA (Fig. 4*K*). We also found matching host responses (BiP induction and sXBP1 levels) at the protein level (Fig. 4*K*, protein quantification of sXBP1 below). For cells infected with VN1203 NS1^{-}, we did not observe induction of ER stress, presumably because the VN1203 NA fails to induce this stress response irrespective of the function of NS1. Unexpectedly, engineered NS1 mutants of the Neth602 strains also behaved like the parental virus with regards to ER stress induction, possibly indicating that this strain has evolved additional uncharacterized inhibitors of this pathway (*SI Appendix*, Fig. S3 *A* and *B*). However, Neth602 NS1^{+} also displayed more NA upon infection, which might shield the results (*SI Appendix*, Fig. S3 *A* and *B*).

In order to delineate whether NS1-dependent antagonism of ER stress by CPSF30 binding depends on the antagonism of type I interferon or is an independent function, we took advantage of A549 cell lines lacking the expression of either the retinoic acid-inducible gene I (RIG-I) or the signal transducer and activator of transcription 1 (STAT1) (*SI Appendix*, Fig. S3*C*). RIG-I is the bona fide cytosolic sensor responsible for the induction of type I interferon expression in IAV-infected epithelial cells. STAT-1 is a key signaling molecule downstream of the IFN type I receptor and directly responsible for the transcription of interferon-stimulated genes (ISGs). Importantly, inhibition of ER stress induction during infection occurs independently of a functional host type I interferon system. Indeed, we observe that both A549 RIG-I$^{-/-}$ and STAT1$^{-/-}$ cells respond with comparable levels of XBP1 splicing as A549 WT to infection with PR8, VN1203, or Neth602 (Fig. 4*L*).

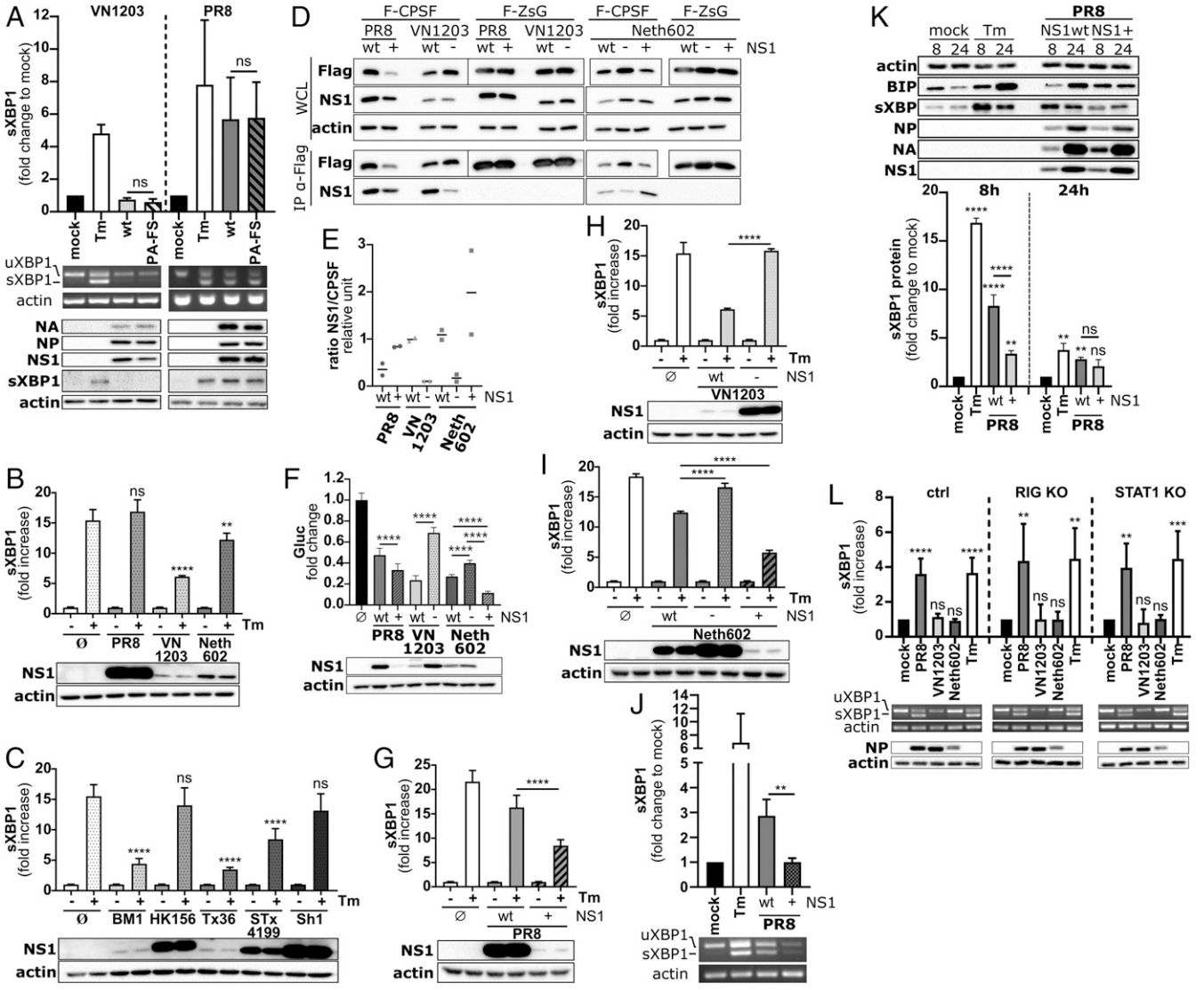

Fig. 4. NS1 prevents UPR, independently of IFN signaling, through its CPSF30 binding ability. (*A*) A549 cells were treated with PBS (mock) or Tm or infected at a MOI of 5 for 8 h with VN1203 or PR8 or the isogenic PA frameshift (PA-FS) mutants ($n = 3$). At 8 h postinfection, cells were lysed and analyzed by semi-quantitative RT-PCR and WB for viral proteins (NA, NP, and NS1) and the cellular proteins (XBP1 and actin). The graph represent mean with SD of the densitometry analysis of the sXBP1 cDNA ($n = 3$) and unpaired *t* test was used to compare WT and mutant viruses. (*B* and *C*) The 293T cells were transfected with pFLAG-XBP1u-FLuc and pCAGGS empty vector (Ø) or pCAGGS encoding NS1 proteins from different viruses: PR8, VN1203, Neth602, BM1, HK156 (A/Hong Kong/156/1997), Tx36, Stx4199 (A/Swine/Texas/4199-2/1998), and Sh1. At 16 h posttransfection, cells were treated with solvent or tunicamycin and lysed 8 h posttreatment. Lysates were subjected to luciferase activity measurement and WB analysis using anti-NS1 antibody. For each condition the luciferase activity of the treated sample was normalized to the untreated. Graphs represent the mean fold increase with SD of triplicate ($n = 2$). One-way ANOVA with Dunnett correction was used to compare treated samples with mock. (*D* and *E*) The 293T cells were transfected with pCAGGS.Flag-CPSF30 (F-CPSF) or pCAGGS.Flag-ZsGreen (F-ZsG) for 24 h prior to infection with either PR8, PR8 NS1^{+}, VN1203, VN1203 NS1^{-}, Neth602, Neth602 NS1^{-}, or Neth602 NS1^{+}. Anti-Flag M2 affinity beads were used to IP the Flag-tagged proteins and their interactors. (*D*) Results were analyzed by WB using anti-Flag antibody and anti-NS1 antibody. (*E*) The amount of NS1 protein bound to Flag-CPSF30 was quantified using densiometric analysis ($n = 2$). (*F*) The 293T cells were transfected with pCMV.Gluc (M60I) and pCAGGS empty vector (Ø) or pCAGGS expressing different NS1 as indicated. Supernatants were subjected to luciferase activity measurement and cell lysates to WB analysis using anti-NS1 antibody. The luciferase activity was normalized to one transfected with the Gluc-expressing plasmid and the empty vector. Graphs represent the mean fold increase with SD of triplicate ($n = 3$). (*G–I*) The 293T cells were transfected with pFLAG-XBP1u-FLuc and pCAGGS empty vector (Ø) or pCAGGS encoding NS1 proteins from different viruses as indicated. At 16 h posttransfection, cells were treated with solvent or tunicamycin and lysed 8 h posttreatment. Lysates were subjected to luciferase activity measurement and WB analysis using anti-NS1 antibody. For each condition the luciferase activity of the treated sample was normalized to the untreated. Graphs represent the mean fold increase with SD of triplicate. Tm-treated conditions were compared using unpaired *t* test in *G* and *H* while we used one-way ANOVA in *I*. (*J* and *K*) A549 cells were treated with PBS (mock) or Tm or infected at a MOI of 2 with PR8 and PR8 NS1^{+} as indicated ($n = 3$). (*J*) Cells were lysed 8 h postinfection and subjected to semiquantitative RT-PCR. The graph represents mean with SD of the densitometry analysis of the sXBP1 cDNA, and unpaired *t* test was used. (*K*) Cells were lysed at the indicated time point and analyzed by WB for host proteins (actin, BiP, and XBP1) and viral proteins (NP, NS1, and NA). Exposures shown are the same for all samples. The WB shown is representative of three experiments. The amount of sXPB1 protein was quantified using densiometric analysis and the graph represents the mean fold increase in XBP1 protein amount over mock with SD. Samples within the same time point were compared using multiple comparison one-way ANOVA with Turkey correction. (*L*) A549 ctrl, RIG1 knockout (KO), and STAT1 KO cells were infected with PR8, VN1203, or Neth602 at a MOI of 5. Cells were lysed 8 h pi and subjected to semi-quantitative RT-PCR and WB analysis. The graph represents mean with SD of the densitometry analysis of the sXBP1 cDNA (for each cell type the results for two clones were pooled, $n = 2$), and one-way ANOVA with Dunnett correction was used to compared each virus with mock within each cell line. ns $P > 0.05$, *$P \leq 0.05$, **$P \leq 0.01$, ***$P \leq 0.001$, ****$P \leq 0.0001$.

These results define an additional role for NS1 in modulating antiviral host responses.

NS1 CPSF30 Binding Ability Confers a Replication Advantage In Vivo and Prevents UPR in Three-Dimensional (3D) Human Epithelial Airways. In order to assess whether the binding of NS1 to CPSF30 confers an overall advantage to the virus in vivo, we inoculated groups of six mice with phosphate buffer saline (PBS) or 40 pfu of PR8 or PR8 NS1$^+$. Mouse weights were monitored daily (Fig. 5*A*) and viral titer was determined on days D2, D4, and D6 pi (Fig. 5*B*). PR8 NS1$^+$ shows a growth advantage from 2 d postinfection (dpi) with this advantage beginning to be statistically significant at 4 and 6 dpi. This replication phenotype was reflected in mice weight. Indeed, mice infected with PR8 NS1$^+$ lost weight faster than the ones infected with PR8 (most prominent at 6 dpi) Our results indicate that the capacity of NS1 to bind and antagonize CPSF30 confers a replicative advantage to the virus in vivo. Mechanistically, data from infected murine lung epithelial cells (LA4) suggest that as in human cells, NS1 binding to CPSF30 reduces the UPR as indicated by specific qPCR for DNAjb9 (mouse homolog to ERdj4) (*SI Appendix*, Fig. S4).

Finally, we tested the NS1 mutant viruses in a stratified primary human airway epithelial cell model, cultured in an air–liquid interface. We infected these cells apically with PR8, PR8 NS1$^+$, VN1203, and VN1203 NS1$^-$. RNA was extracted 24 h pi and processed for RT-qPCR analysis. First, we determined viral replication using M1 cDNA copies as a surrogate marker. Within each virus pair, WT and mutant viruses replicated to the same level (Fig. 5*C*). Then, we performed qPCR for the ER stress–related genes ERdj4, CHOP, and BiP (Fig. 5*D*). In the case of PR8, we observed a differential expression, with those genes being down-regulated during PR8 NS1$^+$ infection compared with PR8. For VN1203, the expression of ERdj4 and BiP are the same for the two viruses, while CHOP expression is slightly increased in VN1203 NS1$^-$ compared with VN1203. Taken together, these data confirm IAV NS1-dependent antagonism of host cell ER stress in a relevant primary human cell model in context of infection.

Discussion

Multiple papers have identified that modification in the glycosylation pattern of the HA have an impact on the host inflammatory response and overall virus virulence in vivo (51, 52). This increased virulence was later linked to ER stress induction. More specifically removing glycosylation sites on HA was associated with higher ER stress levels and higher virulence, while addition of glycosylation sites was associated with reduced ER stress and reduced virulence (21, 22). These results are probably in line with the observation that N-linked glycans are important for glycoprotein stability and folding and that mutants might enter a misfolded state easier (14).

To date, the role of NA in ER stress induction was not investigated. We demonstrate here by combining genetic, biochemical, and cell biological approaches that in fact expression of the minor glycoprotein NA is the major determinant for ER stress induction during IAV infection. In order to assess ER stress response induced by IAV, we largely relied on measurement of XBP1 splicing as a surrogate marker for the overload of the ER protein folding machinery. Indeed, splicing of XBP1 mRNA is a direct readout for IRE1α activation. While we do not believe this diminishes our findings in general, we believe a detailed assessment of the remaining PERK and ATF6 pathways would be of interest.

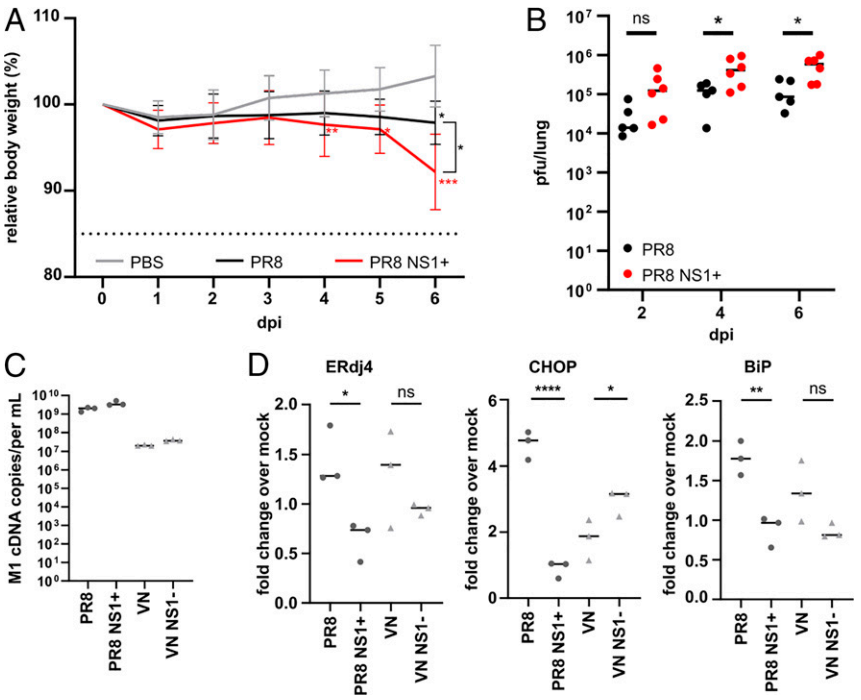

Fig. 5. NS1 CPSF30-binding ability confers an advantage in vivo and prevents UPR in 3D human epithelial airways. (*A* and *B*) Eight-week-old female C57B/6 mice were inoculated with PBS or 40 pfu of PR8 or PR8 NS1$^+$ ($n = 6$ per group). (*A*) Weight was monitored daily and the relative body weight was plotted. Two-way ANOVA (or mixed-effects model) with Turkey's correction was used to compared each group within the same time pi. The dotted line represents the 15% body weight loss defined as the humane endpoint. (*B*) Whole lungs were collected at 2, 4, and 6 dpi and processed for analysis by plaque assay. Viral lung titers are shown in pfu/lung. Each dot represents an individual mouse and the bar represents the mean. Two-way ANOVA (multiple comparisons) with Sidak correction was used to compare each group each day. (*C* and *D*) Three-dimensional epithelial airways were infected apically at a MOI of 5 with PBS, PR8, PR8 NS1$^+$, VN1203, and VN1203 NS1$^-$ ($n = 3$). At 24 h pi, cells were lysed, total cellular RNA was extracted, and samples were processed by RT-qPCR for viral M1 (*C*), and ER stress–related genes (*D*) ERdj4, CHOP, and BiP. Each dot represents a Transwell and the bar represents the median. One-way ANOVA with Sidak correction was used to compare the values. ns $P > 0.05$, *$P \leq 0.05$, **$P \leq 0.01$, ****$P \leq 0.0001$.

Our results implicate that both the quantity of NA and the sequence of the NA protein are essential determinants for NA's specific capacity to induce ER stress. However, from our sample set of viruses we conclude that ER stress leading to a substantial activation of the UPR is rather the exception than the rule in IAV biology. Most IAV strains appear to welcome a low levels of ER stress, potentially for increased glycoprotein folding capacity, while avoiding a full activation of the otherwise potentially deleterious UPR. Additionally, ER stress was recently proposed to increase the tolerance for mutations in the major glycoproteins HA and NA (53). For the virus this is an important escape route to avoid the adaptive immune response of the host. A fine-tuned level of ER stress response might thus be overall beneficial for the virus. In order to achieve this low level of ER stress response, IAV would have in theory three options: 1) reducing the trigger load by reducing overall expression of NA, 2) express an easily foldable NA less recognized by BiP, or 3) antagonizing host glycoprotein production or even host protein production in general. Intriguingly, all strategies seem to be used by IAVs. They even seem to be used in combination as seen for A/Vietnam/1203/2004. Indeed, during infection with the VN1203 strain, little NA is produced despite the fact that the NS1 protein of VN1203 is able to antagonize CPSF30, thus preventing the polyadenylation of newly synthesized host mRNA. However, a true correlation between NA amounts and the capacity of NS1 to antagonize CPSF30 is bioinformatically difficult, since the prediction of ER stress induction potential requires nonavailable data.

Shutdown of host translation by NS1 was so far only associated with antagonism of innate immune responses. Here, we demonstrate in two knockout cell lines of major signaling hubs for anti-IAV responses, that the capacity to temper the ER stress response functions independently of a functional innate immune system. This means that the selection pressure to maintain this function is not only dictated by the innate host response, especially in view of the numerous, apparently redundant strategies the virus developed to counteract innate immunity. Additionally, NS1 is described to target protein kinase activated by dsRNA (PKR) a second signaling hub downstream of ER stress responses, which might also contribute to control host protein synthesis (54, 55).

Many viruses, both RNA and DNA, have been described to subvert the ER stress response to the best of their advantage (56). Viruses have evolved mechanisms to antagonize, induce, or even keep the ER stress response under tight control. A good example of this fine-tuned balance was recently described for Kaposi's sarcoma–associated herpesvirus (KSHV). Indeed, KSHV activates the UPR sensors but inhibits accumulations of downstream transcription factors (57). Murine cytomegalovirus (MCMV) was also recently shown to activated ER stress, since it requires the transcription factor sXBP1 and AT6 for the expression of its viral immediate early genes (58). Interestingly, herpes simplex virus 1 (HSV-1) has evolved a way to suppress IREα signaling. Indeed, Zhang et al. showed that the tegument host shutoff protein UL41 degrades XBP1 mRNA via its endoribonuclease activity (59). This strategy, reducing the total amount of XBP1 mRNA, is fairly similar to the one we described in this paper for IAV. For influenza B, C, and D viruses, no shutoff activity was described for their NS1 proteins (60). It would be of interest to investigate whether these cousins of IAV developed alternative strategies to inhibit ER stress and/or keep it at a tolerable level.

In summary, we demonstrated here that IAV NA is the major determinant of ER stress induction during viral infection and that inhibition of cellular mRNA polyadenylation by NS1 is an important control mechanism to fine tune this proapoptotic host response to the virus advantage.

Materials and Methods

Materials Availability. All unique/stable reagents generated in this study are available from the lead contact with a completed Materials Transfer Agreement.

Cells. A549 (adenocarcinomic human alveolar basal epithelial cells, ATCC) and A549-derived cell lines were grown in DMEM/F12 (Dulbecco's Modified Eagle Medium: Nutrient Mixture F-12, Gibco). HEK 293T (human embryonic kidney, ATCC) and MDCK (Madin-Darby canine kidney, ATCC) cells were grown in DMEM. LA4 (murine epithelial lung adenoma, ATCC) cells were grown in DMEM/F12 supplemented with 15% foetal bovine serum (FBS). Cell culture media were supplemented with 10% (vol/vol) heat-inactivated FBS (Gibco) and 100 U/mL penicillin/streptomycin (Pen/Strep). Cells were maintained at 37 °C with 5% CO_2 and 90% humidity. RIG-1 and STAT1 knockout A549 clones were generated by the means of CRISPR–Cas9-mediated genome editing using ribonucleoproteins (RNPs) consisting of Alt-R *Sp*Cas9 nuclease in complex with Alt-R CRISPR–Cas9 CRISPR RNA (crRNA) (RIG-1 protospacer domain targeted in RIG-1 KO-1 clone, CCACCGAGCAGCGACGCAGCCTG, RIG-1 protospacer domain targeted in RIG-1 KO-2 clone: AAACAACAAGGGCCCAATGGAGG; STAT1 protospacer domain targeted in both STAT1 KO-1 and -2, TCAGACAGTACCTGGCACAGTGG, underlined the NGG:). TracerRNA, crRNA oligos, and recombinant Cas9 endonuclease were obtained from Integrated DNA Technology. In brief, preassembled RNP complexes were delivered into A549 cells by reverse transfection, using RNAiMax (Thermo Fisher Scientific). At 48 h posttransfection, cells were subjected to T7 endonuclease I (New England Biolabs) assay to estimate the frequency of genome-editing events. Screening of individual clones, generated by limiting dilution, was performed by immunoblotting to determine the protein expression of the target genes, followed by genotyping by next-generation sequencing (NGS) or Sanger sequencing. Of note, matching control lines were subjected to the same protocol, but carried no InDel mutations.

Plasmids. Plasmids are listed in *SI Appendix*, Table S4.

Antibodies. Antibodies for immunoblotting and immunofluorescence are listed in *SI Appendix*, Table S5.

Oligonucleotides. All oligonucleotides were purchased from Microsynth (France) represented in *SI Appendix*, Table S6.

Viruses. Virus stocks were grown in MDCK II cells or embryonated chicken eggs (*SI Appendix*, Table S7). For virus infections, cells were washed once in PBS, viruses were diluted in PBS-0.2% bovine serum albumin (BSA) and added to cell monolayer. At 45 min pi, cells were washed once with PBS and 1 mL of infection media was added (DMEM/F12 with 0.2% BSA and 1% Pen/Strep). Recombinant viruses were produced using the eight-plasmid rescue system (61). Unique viral clones were isolated after plaque assay on MDCK, grown in eggs or cells, and their genome fully sequenced.

Immunofluorescence, Z-Stack Imaging, and Analysis. A549 cells were infected with PR8 at a MOI of 5 for 8 h or 24 h, treated with PBS or tunicamycin at 5 μg/mL. Cells were fixed in 4% formaldehyde for 20 min and blocked in PBS 1% BSA for 1 h. Then cells were stained with primary/secondary antibody pairs depending on the experiment: Anti-BIP and secondary anti-rabbit Alexa Fluor 488, anti-CD44 and secondary anti-rat Alexa Fluor 555, mouse anti-NP, and secondary anti-mouse Alexa Fluor 633 or rabbit anti-NP and secondary anti-rabbit Alexa Fluor 488.

Widefield images were acquired using a Nikon Eclipse ts2R microscope and Nis-Elements BR v4.60 software. Confocal images were acquired using a Zeiss LSM 800 Airyscan confocal laser scanning microscope with ZEN 2.3 software and a Plan Apochromat 63× 1.4 NA objective with oil immersion. The fluorophores DAPI, AF-488, AF-555, and AF-633 were excited by 405-, 488-, 561-, and 640-nm laser lines, respectively. Pinhole diameters, detector gains, and laser intensities were optimized thanks to the bioimaging staff and kept constant throughout the same experiment. Cells with few neighboring cells were selected for image acquisition in order to facilitate the delimitation of a single cell in the following image analysis step. For the infected conditions, cells were screened for infection with the 640-nm track prior to imaging. Z-stacks were acquired using three tracks, 405, 488, and 561 nm.

XBP1 mRNA Splicing Assay Using Semiquantitative RT-PCR. Following infection, total cellular RNA was isolated using the E.Z.N.A. Total RNA kit (Omega Bio-Tek #R6834-01) according to the manufacturer's instructions. cDNA was synthetized using M-MLV reverse transcriptase (Promega #M170A) according to the manufacturer's instructions but using 100 ng of RNA as starting material and oligo dT as primers. PCR was performed using GoTaq G2 DNA polymerase (Promega #M784B) with 5× Green GoTaq reaction buffer (Promege #M791A). The primers were designed to flank the splicing site of the XBP1 mRNA in order to amplify both the unspliced and the spliced form. A PCR for β-actin was used as a control. PCR products were separated on a 3% agarose

gel containing EtBr for visualization. Images were acquired using the GelDoc XR+ System (Bio-Rad) and analyzed with Image Lab software (v4.1 from Bio-Rad).

XBP1 mRNA Splicing Using Luciferase Reporter. Subconfluent 293T cells were transfected (using TransIT-LT1, Mirus #Mir2304) with pFLAG-XBP1u-FLuc (39). Cells were also transfected with other expression plasmids (pCAGGS constructs expressing either influenza NA or NS1, or pcDNA3.1(+)-GRP78/BiP expressing the chaperone BiP) and treated or not with tunicamycin (Merck #T7765) at 1 μg/mL or kifunensine (Merck #K1140) at 10 μg/mL. At the indicated time, cells were lysed and the luciferase assay was performed using a dual-luciferase reporter assay system (Promega #E1910).

Enzyme-Like Lectin Assay. The neuraminidase activity was quantified using a lectin (peanut agglutinin, PNA) linked to a peroxidase (Po-PNA), described by Lambré et al. (62). Fetuin 50 μg/mL (Merck #F3385) in 0.1 M carbonate/bicarbonate buffer pH 9.6 was coated on a high-protein binding plate (Nunc MaxiSorp # 44-2404-21) overnight at 4 °C. Plates were washed three times with PBS, blocked with PBS 5% BSA for 1 h and then washed three times in PBS 0.5% Tween-20. For NA activity, 100 μL of serial dilution of viruses or purified proteins were added to the fetuin-coated plate and incubated for 2 h at 37 °C. For viruses, the starting concentration was 10^7 pfu/mL in PBS-CaCl2-MgCl2 (Gibco #14040091) with 1% BSA followed by a threefold dilution. For purified proteins (63), the starting concentration was 100 ng/mL in PBS-CaCl2-MgCl2 with 1% BSA followed by a twofold dilution. Plates were washed six times in PBS 0.5% Tween-20 and then 100 μL of Po-PNA (Merck #L7759) at 5 μg/mL diluted in PBS was added for 2 h at room temperature and in the dark. Plates were washed six times in PBS 0.5% Tween-20, and 100 μL of TMB (3,3′,5,5′-tetramethylbenzidine, Merck #860336) was added. After a 1- to 5-min incubation, the reaction was stopped using 50 μL of 2 M sulfuric acid. Plates were read at 450 nm using a BioTek Synergy H1 plate reader.

Immunoprecipitation Assay. The 293T cells were transfected with 1 μg of pCAGGS.Flag-CPSF30 or with 0.5 μg of pCAGGS.Flag-ZsGreen using 2 μL/μg DNA of TransIT-LT1 (Mirus #Mir2304). At 24 h posttransfection, cells were infected at a MOI of either 5 (for PR8 and VN1203) or 0.5 (for Neth602). For PR8 and VN1203, cells were lysed on ice after 8 h in 300 μL IP lysis buffer (50 mM Tris HCl pH 7.5, 150 mM NaCl, 0.5% vol/vol Nonidet P-40, 5 mM EDTA with protease inhibitors) (Pierce #88266). For Neth602 infection, cells were lysed after 24 h. Fifty microliters of the cleared lysate was mixed 1:1 with protein lysis buffer (50 mM Tris HCL pH 6.8, 10% glycerol, 2% SDS, 0.1 M DTT and 0.1% bromophenol blue in H_2O) to serve as whole cell lysate control, while the remaining 200 μL was processed for immunoprecipitation at 4 °C using anti-Flag M2 affinity gel (Sigma #A2220). Samples were then used in a Western blot.

Gaussia Luciferase Assay. Subconfluent 293T cells were transfected (using TransIT-LT1, Mirus #Mir2304) with pCMV.Gluc (M60I). This construct expresses Gaussia luciferase under the control of a CMV promoter. Cells were also transfected with other expression plasmids for NS1 (pCAGGS constructs expressing different NS1 proteins). At 24 h posttransfection, culture media were collected and frozen at −20 °C. At the same time, cells were lysed for subsequent WB analysis.

RT-qPCR. cDNA was synthetized using M-MLV reverse transcriptase (Promega #M170A) according to the manufacturer's instructions, using 100 ng of RNA as starting material and oligo dT as primers. For quantitative PCR, 1 μL of cDNA was mixed with 10 μL of 2X KAPA SYBR FAST Universal (#KK4602), 0.4 μL of each forward (10 μM) and reverse (10 μM) primer, and 8.2 μL of UltraPure DNase/RNase free distilled water (Invitrogen #10977). qPCR was performed on a BioRad CFX96 Real-Time System with the following protocol: initial denaturation step at 95 °C for 5 min, followed by 40 cycles of denaturation at 95 °C for 30 s, and annealing/extension at 60 °C for 30 s.

Structural Modeling. The models of neuraminidases of different influenza strains were calculated with Modeler 9.18 (64). The used templates and the sequence similarity are presented in *SI Appendix*, Table S8. For each protein the 500 models were calculated that were subsequently assessed by the discrete optimized protein energy (DOPE) method (65). The visual inspection and assessment of secondary structural elements were done on models with the best DOPE score using Chimera software (66). The BiPPred server was used to evaluate the probability of BiP protein binding to the different peptides on the sequences of NA (47). The sequences of the N-terminal fragments and of the loop are included in the analysis are shown in *SI Appendix*, Tables S1 and S2, respectively.

Infection of 3D Human Upper Airway Epithelium. The 3D human upper airway epithelium (MucilAir) from a pool of healthy donors was purchased from Epithelix and cultured in an air–liquid interface. Cells were infected after six washes with PBS Ca^{+2} Mg^{+2} with 100 μL of virus suspension (MOI 5) from the apical side. Virus was removed after 3 h and Transwells were incubated for an additional 21 h at 37 °C. RNA was isolated 24 h pi, using E.Z.N.A. Total RNA kit (Omega Bio-Tek #R6834-01) according to the manufacturer's instructions.

Mice and Viral Lung Titer. C57BL/6J mice (female, 8 wk of age) were purchased from Charles River Laboratories and housed under SPF/BSL2 conditions. All animals were housed for 7 d to adjust to housing conditions under a strict 12 h light/dark cycle and fed ad libitum. For IAV infection, mice were injected intraperitoneally with a mix of ketamin/xylazine (100 and 5 mg/kg, respectively) in 100 μL of sterile PBS. Upon reaching deep anesthesia, mice were inoculated intranasally with 40 μL of PBS or with 40 μL of PBS containing 40 pfu of virus. Animal weights were measured daily. Animals were killed using controlled CO_2 exposure at 2, 4, and 6 dpi. Whole lungs were sampled immediately after killing using sterile tools. Tools were changed in between experimental groups to avoid cross-contamination. Whole lungs were homogenized with 1/4 inch stainless steel grinding balls (MPBio) in 1 mL PBS, using a Bead Blaster 24 (Benchmark Scientific) with a speed setting of 6 m/s for 30 s and 30-s intervals, repeated two times. Samples were centrifuged at 2,000 × *g* for 5 min and supernatant was used for plaque assay in MDCK cells.

Plaque Assay. A confluent monolayer of MDCK cells was infected with 200 μL of serially diluted virus. Viruses were diluted in PBS 0.2% (wt/vol) bovine serum albumin (BSA) (Millipore; 126579). Forty-five minutes pi, the inoculum was removed and an agarose overlay (final concentrations: 1× minimal essential medium [MEM], 1% agarose, 100 mM l-glutamine, 2.5% sodium bicarbonate, 0.5 M Hepes, 5 mg/mL of Pen/Strep, 0.2% BSA, and 0.01% diethylaminoethyl-dextran) was added. Cells were incubated at 37 °C for 48 h. Then cells were fixed in formaldehyde, the overlay was removed, and the cell monolayer was stained with a solution of crystal violet.

Statistics. Statistical analysis was performed using GraphPad Prism 8. Statistical tests applied are indicated in each respective figure legend. ns $P > 0.05$, $*P \leq 0.05$, $**P \leq 0.01$, $***P \leq 0.001$, $****P \leq 0.0001$.

Ethical Approval. All animal procedures were in accordance with federal regulations of the Bundesamt für Lebensmittelsicherheit und Veterenärwesen (BLV), Switzerland (Tierschutzgesetz) and approved by direction de l'expérimentation animale and the cantonal authorities of the Canton Geneve (license number GE/92/15). Embryonated chicken eggs were obtained from the University of Geneva Animalerie d'Arare and infected on day 10 of embryonic development.

Data Availability. All study data are included in the article and/or supporting information.

ACKNOWLEDGMENTS. This work was supported by the Swiss National Science Foundation through Grants 182475 to M.S. and 182464 to B.G.H. and by the Gertrude von Meissner Foundation. Molecular graphics and analyses were performed with University of California San Francisco (UCSF) Chimera, developed by the Resource for Biocomputing, Visualization, and Informatics at UCSF, with support from NIH Grant P41-GM103311. We thank the Protein Modelling Unit of the University of Lausanne for structural bioinformatics support.

1. K. W. Moremen, M. Tiemeyer, A. V. Nairn, Vertebrate protein glycosylation: Diversity, synthesis and function. *Nat. Rev. Mol. Cell Biol.* **13**, 448–462 (2012).
2. A. Bakunts *et al.*, Ratiometric sensing of BiP-client versus BiP levels by the unfolded protein response determines its signaling amplitude. *eLife* **6**, e27518 (2017).
3. M. Vitale *et al.*, Inadequate BiP availability defines endoplasmic reticulum stress. *eLife* **8**, e41168 (2019).
4. K. F. R. Pobre, G. J. Poet, L. M. Hendershot, The endoplasmic reticulum (ER) chaperone BiP is a master regulator of ER functions: Getting by with a little help from ERdj friends. *J. Biol. Chem.* **294**, 2098–2108 (2019).
5. P. Walter, D. Ron, The unfolded protein response: From stress pathway to homeostatic regulation. *Science* **334**, 1081–1086 (2011).
6. H. Yoshida, T. Matsui, A. Yamamoto, T. Okada, K. Mori, XBP1 mRNA is induced by ATF6 and spliced by IRE1 in response to ER stress to produce a highly active transcription factor. *Cell* **107**, 881–891 (2001).
7. K. Yamamoto, H. Yoshida, K. Kokame, R. J. Kaufman, K. Mori, Differential contributions of ATF6 and XBP1 to the activation of endoplasmic reticulum stress-responsive cis-acting elements ERSE, UPRE and ERSE-II. *J. Biochem.* **136**, 343–350 (2004).

8. A. H. Lee, N. N. Iwakoshi, L. H. Glimcher, XBP-1 regulates a subset of endoplasmic reticulum resident chaperone genes in the unfolded protein response. *Mol. Cell. Biol.* **23**, 7448–7459 (2003).
9. R. Iurlaro, C. Muñoz-Pinedo, Cell death induced by endoplasmic reticulum stress. *FEBS J.* **283**, 2640–2652 (2016).
10. W. Chen, J. Helenius, I. Braakman, A. Helenius, Cotranslational folding and calnexin binding during glycoprotein synthesis. *Proc. Natl. Acad. Sci. U.S.A.* **92**, 6229–6233 (1995).
11. D. N. Hebert, B. Foellmer, A. Helenius, Calnexin and calreticulin promote folding, delay oligomerization and suppress degradation of influenza hemagglutinin in microsomes. *EMBO J.* **15**, 2961–2968 (1996).
12. N. Wang, E. J. Glidden, S. R. Murphy, B. R. Pearse, D. N. Hebert, The cotranslational maturation program for the type II membrane glycoprotein influenza neuraminidase. *J. Biol. Chem.* **283**, 33826–33837 (2008).
13. C. F. Basler, A. García-Sastre, P. Palese, Mutation of neuraminidase cysteine residues yields temperature-sensitive influenza viruses. *J. Virol.* **73**, 8095–8103 (1999).
14. R. Daniels, B. Kurowski, A. E. Johnson, D. N. Hebert, N-linked glycans direct the cotranslational folding pathway of influenza hemagglutinin. *Mol. Cell* **11**, 79–90 (2003).
15. M. S. Segal, J. M. Bye, J. F. Sambrook, M.-J. H. Gething, Disulfide bond formation during the folding of influenza virus hemagglutinin. *J. Cell Biol.* **118**, 227–244 (1992).
16. U. Tatu, C. Hammond, A. Helenius, Folding and oligomerization of influenza hemagglutinin in the ER and the intermediate compartment. *EMBO J.* **14**, 1340–1348 (1995).
17. T. Saito, G. Taylor, R. G. Webster, Steps in maturation of influenza A virus neuraminidase. *J. Virol.* **69**, 5011–5017 (1995).
18. D. V. da Silva, J. Nordholm, U. Madjo, A. Pfeiffer, R. Daniels, Assembly of subtype 1 influenza neuraminidase is driven by both the transmembrane and head domains. *J. Biol. Chem.* **288**, 644–653 (2013).
19. B. Hogue, D. Nayak, Synthesis and processing of the influenza virus neuraminidase, a type II transmembrane glycoprotein. *Virology* **188**, 510–517 (1992).
20. S. M. Hurtley, D. G. Bole, H. Hoover-Litty, A. Helenius, C. S. Copeland, Interactions of misfolded influenza virus hemagglutinin with binding protein (BiP). *J. Cell Biol.* **108**, 2117–2126 (1989).
21. E. R. Hrincius *et al.*, Acute lung injury results from innate sensing of viruses by an ER stress pathway. *Cell Rep.* **11**, 1591–1603 (2015).
22. Y. Yin *et al.*, Glycosylation deletion of hemagglutinin head in the H5 subtype avian influenza virus enhances its virulence in mammals by inducing endoplasmic reticulum stress. *Transbound. Emerg. Dis.* **67**, 1492–1506 (2020).
23. I. H. Hassan *et al.*, Influenza A viral replication is blocked by inhibition of the inositol-requiring enzyme 1 (IRE1) stress pathway. *J. Biol. Chem.* **287**, 4679–4689 (2012).
24. E. C. Roberson *et al.*, Influenza induces endoplasmic reticulum stress, caspase-12-dependent apoptosis, and c-Jun N-terminal kinase-mediated transforming growth factor-β release in lung epithelial cells. *Am. J. Respir. Cell Mol. Biol.* **46**, 573–581 (2012).
25. D. A. Frabutt, B. Wang, S. Riaz, R. C. Schwartz, Y.-H. Zheng, Innate sensing of influenza A virus hemagglutinin glycoproteins by the host endoplasmic reticulum (ER) stress pathway triggers a potent antiviral response via ER-associated protein degradation. *J. Virol.* **92**, e01690–17 (2018).
26. Y. Sun *et al.*, Molecular basis for the recognition of the human AAUAAA polyadenylation signal. *Proc. Natl. Acad. Sci. U.S.A.* **115**, E1419–E1428 (2018).
27. L. Schönemann *et al.*, Reconstitution of CPSF active in polyadenylation: Recognition of the polyadenylation signal by WDR33. *Genes Dev.* **28**, 2381–2393 (2014).
28. M. E. Nemeroff, S. M. Barabino, Y. Li, W. Keller, R. M. Krug, Influenza virus NS1 protein interacts with the cellular 30 kDa subunit of CPSF and inhibits 3'end formation of cellular pre-mRNAs. *Mol. Cell* **1**, 991–1000 (1998).
29. K. Y. Twu, D. L. Noah, P. Rao, R. L. Kuo, R. M. Krug, The CPSF30 binding site on the NS1A protein of influenza A virus is a potential antiviral target. *J. Virol.* **80**, 3957–3965 (2006).
30. I. Ramos *et al.*, Contribution of double-stranded RNA and CPSF30 binding domains of influenza virus NS1 to the inhibition of type I interferon production and activation of human dendritic cells. *J. Virol.* **87**, 2430–2440 (2013).
31. G. Kochs, A. García-Sastre, L. Martínez-Sobrido, Multiple anti-interferon actions of the influenza A virus NS1 protein. *J. Virol.* **81**, 7011–7021 (2007).
32. B. G. Hale *et al.*, Inefficient control of host gene expression by the 2009 pandemic H1N1 influenza A virus NS1 protein. *J. Virol.* **84**, 6909–6922 (2010).
33. M. D. Shoulders *et al.*, Stress-independent activation of XBP1s and/or ATF6 reveals three functionally diverse ER proteostasis environments. *Cell Rep.* **3**, 1279–1292 (2013).
34. L. Plate *et al.*, Small molecule proteostasis regulators that reprogram the ER to reduce extracellular protein aggregation. *eLife* **5**, e15550 (2016).
35. H. Yang, M. Niemeijer, B. van de Water, J. B. Beltman, ATF6 is a critical determinant of CHOP dynamics during the unfolded protein response. *iScience* **23**, 100860 (2020).
36. H. Quan, Q. Fan, C. Li, Y. Y. Wang, L. Wang, The transcriptional profiles and functional implications of long non-coding RNAs in the unfolded protein response. *Sci. Rep.* **8**, 4981 (2018).
37. E. C. Hutchinson *et al.*, Conserved and host-specific features of influenza virion architecture. *Nat. Commun.* **5**, 4816 (2014).
38. A. Zheng *et al.*, Enhancing neuraminidase immunogenicity of influenza A viruses by rewiring RNA packaging signals. *J. Virol.* **94**, e00742-20 (2020).
39. J. R. Jheng, K. S. Lau, W. F. Tang, M. S. Wu, J. T. Horng, Endoplasmic reticulum stress is induced and modulated by enterovirus 71. *Cell. Microbiol.* **12**, 796–813 (2010).
40. H. L. Yen *et al.*, Importance of neuraminidase active-site residues to the neuraminidase inhibitor resistance of influenza viruses. *J. Virol.* **80**, 8787–8795 (2006).
41. X. Zhu *et al.*, Influenza virus neuraminidases with reduced enzymatic activity that avidly bind sialic acid receptors. *J. Virol.* **86**, 13371–13383 (2012).
42. Q. Li *et al.*, Structural and functional characterization of neuraminidase-like molecule N10 derived from bat influenza A virus. *Proc. Natl. Acad. Sci. U.S.A.* **109**, 18897–18902 (2012).
43. X. Zhu *et al.*, Crystal structures of two subtype N10 neuraminidase-like proteins from bat influenza A viruses reveal a diverged putative active site. *Proc. Natl. Acad. Sci. U.S.A.* **109**, 18903–18908 (2012).
44. J. M. Brunner *et al.*, Morbillivirus glycoprotein expression induces ER stress, alters Ca2+ homeostasis and results in the release of vasostatin. *PLoS One* **7**, e32803 (2012).
45. J. Hwang, L. Qi, Quality control in the endoplasmic reticulum: Crosstalk between ERAD and UPR pathways. *Trends Biochem. Sci.* **43**, 593–605 (2018).
46. A. D. Elbein, J. E. Tropea, M. Mitchell, G. P. Kaushal, Kifunensine, a potent inhibitor of the glycoprotein processing mannosidase I. *J. Biol. Chem.* **265**, 15599–15605 (1990).
47. M. Schneider *et al.*, BiPPred: Combined sequence- and structure-based prediction of peptide binding to the Hsp70 chaperone BiP. *Proteins* **84**, 1390–1407 (2016).
48. A. E. Firth *et al.*, Ribosomal frameshifting used in influenza A virus expression occurs within the sequence UCC_UUU_CGU and is in the +1 direction. *Open Biol.* **2**, 120109 (2012).
49. B. W. Jagger *et al.*, An overlapping protein-coding region in influenza A virus segment 3 modulates the host response. *Science* **337**, 199–204 (2012).
50. R. L. Kuo, R. M. Krug, Influenza a virus polymerase is an integral component of the CPSF30-NS1A protein complex in infected cells. *J. Virol.* **83**, 1611–1616 (2009).
51. Y. Zhang *et al.*, Glycosylation on hemagglutinin affects the virulence and pathogenicity of pandemic H1N1/2009 influenza A virus in mice. *PLoS One* **8**, e61397 (2013).
52. X. Sun *et al.*, N-linked glycosylation of the hemagglutinin protein influences virulence and antigenicity of the 1918 pandemic and seasonal H1N1 influenza A viruses. *J. Virol.* **87**, 8756–8766 (2013).
53. A. M. Phillips *et al.*, Enhanced ER proteostasis and temperature differentially impact the mutational tolerance of influenza hemagglutinin. *eLife* **7**, e38795 (2018).
54. Y. Lu, M. Wambach, M. G. Katze, R. M. Krug, Binding of the influenza virus NS1 protein to double-stranded RNA inhibits the activation of the protein kinase that phosphorylates the eIF-2 translation initiation factor. *Virology* **214**, 222–228 (1995).
55. J. Y. Min, S. Li, G. C. Sen, R. M. Krug, A site on the influenza A virus NS1 protein mediates both inhibition of PKR activation and temporal regulation of viral RNA synthesis. *Virology* **363**, 236–243 (2007).
56. J. R. Jheng, J. Y. Ho, J. T. Horng, ER stress, autophagy, and RNA viruses. *Front. Microbiol.* **5**, 388 (2014).
57. B. P. Johnston, E. S. Pringle, C. McCormick, KSHV activates unfolded protein response sensors but suppresses downstream transcriptional responses to support lytic replication. *PLoS Pathog.* **15**, e1008185 (2019).
58. F. Hinte, E. van Anken, B. Tirosh, W. Brune, Repression of viral gene expression and replication by the unfolded protein response effector XBP1u. *eLife* **9**, e51804 (2020).
59. P. Zhang, C. Su, Z. Jiang, C. Zheng, Herpes simplex virus 1 UL41 protein suppresses the IRE1/XBP1 signal pathway of the unfolded protein response via its RNase activity. *J. Virol.* **91**, e02056-16 (2017).
60. A. Nogales *et al.*, Functional characterization and direct comparison of influenza A, B, C, and D NS1 proteins in vitro and in vivo. *Front. Microbiol.* **10**, 2862 (2019).
61. M. Quinlivan *et al.*, Attenuation of equine influenza viruses through truncations of the NS1 protein. *J. Virol.* **79**, 8431–8439 (2005).
62. C. R. Lambré, H. Terzidis, A. Greffard, R. G. Webster, Measurement of anti-influenza neuraminidase antibody using a peroxidase-linked lectin and microtitre plates coated with natural substrates. *J. Immunol. Methods* **135**, 49–57 (1990).
63. I. Margine, P. Palese, F. Krammer, Expression of functional recombinant hemagglutinin and neuraminidase proteins from the novel H7N9 influenza virus using the baculovirus expression system. *J. Vis. Exp.*, e51112 10.3791/51112 (2013).
64. B. Webb, A. Sali, Comparative protein structure modeling using Modeller. *Curr. Protoc. Bioinform.* **54**, 5.6.1–5.6.37 (2016).
65. M. Y. Shen, A. Sali, Statistical potential for assessment and prediction of protein structures. *Protein Sci.* **15**, 2507–2524 (2006).
66. E. F. Pettersen *et al.*, UCSF Chimera–A visualization system for exploratory research and analysis. *J. Comput. Chem.* **25**, 1605–1612 (2004).